Precision assessment of label-free psoriasis biomarkers with ultra-broadband optoacoustic mesoscopy

Juan Aguirre[1], Mathias Schwarz [1],Natalie Garzorz[2], Murad Omar[1], Andreas Buehler[1], Kilian Eyerich[2], Vasilis Ntziachristos[1]*

1. Chair for Biological Imaging, Technische Universität München and Institute for Biological and Medical Imaging, Helmholtz Zentrum München,IngolstädterLandstr.1, D85764 Neuherberg, Germany.

2. Division of Environmental Dermatology and Allergy, Helmholtz Center Munich/Technische Universität Munich and ZAUM —Center for Allergy and Environment, Technische Universität Munich, Munich, Germany.

**Corresponding author*
Vasilis Ntziachristos, Ph.D., Professor
Chair for Biological Imaging, Munich School of Bioengineering
Technical University Munich Ismaningerstr. 22, 81675 München Germany
Institute for Biological and Medical Imaging, Helmholtz Zentrum München, IngolstädterLandstr.1, D85764 Neuherberg Germany
Phone: 49-89-31873852;
Fax: 49-89-3187173852 ;
E-mail: v.ntziachristos@tum.de

Imaging plays a critical role in the diagnosis and assessment of dermatological conditions. However, optical or optoacoustic microscopy techniques are limited to visualizing superficial skin features owing to strong photon scattering, whereas ultrasound methods, which can probe deeper seated tissue, lack the contrast to image pathophysiological mechanisms in detail. Here, we demonstrate that raster scan optoacoustic mesoscopy (RSOM) implemented in ultra-wideband (10–180 MHz) detection mode bridges the depth capabilities of ultrasound and the resolution range and high contrast of optical methods in clinical dermatology. By using tomographic reconstruction and frequency equalization to represent low and high spatial-frequency components, we visualize skin morphology and vascular patterns in the dermis and sub-dermis of psoriasis patients, enabling quantification of inflammatory and other biomarkers of psoriasis without the need for contrast agents. Implemented in a handheld device, we showcase how label-free RSOM biomarkers correlate with clinical score and the potential to assess a larger spectrum of skin diseases in research and the clinic.

Psoriasis is a chronic inflammatory skin disease with adverse effects on quality of life and the socio-economical system[1,2]. Current progress in understanding disease pathogenesis reveals that immune dysregulation of T helper 17 cells results in a hyper-proliferative and metabolically activated epidermis[3], manifested as red patches with silver scales. The disease phenotype exhibits increased mitotic rate of keratinocytes, thickening of the stratum spinosum (acanthosis) and strong inflammatory cellular infiltrate consisting of T cells, macrophages and dendritic cells[1]. Moreover, the dermal areas of psoriatic skin are marked with increased vascularization and an increase of tortuous capillaries in the upper dermis[1,4] Nevertheless, many aspects of the psoriasis pathogenesis remain poorly understood. Moreover, lack of biomarkers and objective methods to phenotype the heterogeneous presentation of psoriasis challenges prediction of a therapeutic strategy outcome for individual patients [3].

The psoriatic skin is clinically assessed with the Psoriasis Area Severity Index (PASI)[5], calculated by scoring the appearance of lesion redness, plaque thickness, scaling and percentage of the body affected. PASI is nevertheless subjective and does not assess subsurface features, such as general morphology, vasculature or angiogenesis[6,7], even though the release of growth factors (Vascular Endothelial Growth Factor, Epidermal Growth Factors, Transforming Growth Factor Beta) and changes in vascular architecture are identified as a major hallmark of psoriatic inflammation and typically associated with disease progression[8,4].

Confocal or two-photon microscopy have been considered for skin visualization but only assess depths of a few hundred microns, not appropriate for the thickened psoriatic epidermis[9,10]. Optical Coherence Tomography (OCT) may provide skin morphology images 1-2 mm deep in skin at ~1300 nm [11,12], but imaging of vascular networks observed with flow-sensitive techniques in the visible [13,14] is limited to depths of ~400 μm[15]. Moreover, inherent image artifacts in the axial direction have not been yet addressed and compromise

74 the OCT ability to obtain cross sectional images. Alternatively, high-frequency ultrasound penetrates several
75 millimeters in skin tissue. However, images have strong speckle effects and do not visualize sub-100μm
76 diameter vessels, unless contrast agents (microbubbles) are employed[16], imposing limitations for routine
77 longitudinal application in humans. Moreover, ultrasonic contrast has reduced sensitivity to
78 pathophysiological changes and the study of inflammation or angiogenesis[17]. Therefore, studies of subsurface
79 skin patho-physiology and longitudinal observations are limited by the *in-vivo* imaging tools available today[9,8].
80
81 We present a different perspective in skin imaging by developing portable ultra-broadband (10-180MHz)
82 raster scan optoacoustic mesoscopy (UB-RSOM) and investigate the relation of the imaging features offered in
83 psoriasis and other dermatology applications to pathophysiological metrics of disease. Conventional
84 ultrasound and optoacoustic imaging utilize frequencies over a narrow *band* (e.g. 5-20MHz), which defines
85 the resolution-range and overall image quality achieved. Conversely, UB-RSOM implements ultra-short
86 photon pulses (<2ns) that excite an ultra-broad ultrasound frequency spectrum. Central to achieving high-
87 performance UB imaging is the use of focused Lithium niobate crystal (LiNbO3) detection of optoacoustic
88 signals at high-numerical aperture (NA>60^0) yielding detection bandwidths of 10-180Mhz. We investigated
89 features offered by UB-RSOM in skin and skin disease and developed Frequency Band Equalization (FBE) to
90 effectively utilize the broad frequency content. We demonstrate the visualization of pathophysiological skin
91 features *in vivo* in label-free mode, which has not been achieved by other imaging modalities. We discover
92 how tomographic reconstruction of absorption contrast can quantify critical dermatology sub-surface features
93 associated with dermal angiogenesis and skin inflammation, without using contrast agents and the highest
94 resolution to depth ratio reported in label-free mode. We further devise an UB-RSOM index of skin conditions
95 aiming to offer a quantitative metric of disease severity in the context of precision medicine requirements, and
96 compare it to clinical score. We discuss how the method can advance the study and quantification of
97 dermatological conditions and response to treatment.

RESULTS

Qualitative evaluation of the optoacoustic mesoscopy skin imaging performance

Developed for portable skin imaging, (**see Fig. 1a-c and methods**), UB-RSOM respected the American National Standard for Safe Use of Lasers (ANSI) safety limits for human use (**see methods**). Handheld operation was achieved by designing a compact scan head (see methods) that employed fixed illumination to overcome image artifacts arising from spatially-dependent optical-fluence variations common to raster scan implementations that move in tandem both the sound detector and the illuminator [18].

Detected signals were reconstructed and were separated in two frequency bands, typically 10-60MHz (**Fig.1d**) and 60-180MHz (**Fig.1e)**; or alternatively 10-42 MHz and 42-120MHz bands(see **methods and Suppl. Fig. 1**). A low-frequency band image (rendered in red color) and a high-frequency band image (rendered in green color) were correspondingly reconstructed, frequency equalized (**see methods**) and co-registered (**Fig.1d-f**). This operation allows rendering of fine spatial details together with lower resolution skin structures, the latter typically of higher intensity. Images from healthy volunteers were collected from areas spanning 8x2mm^2 (80 sec. scan time) to 8x8mm^2 (320 sec. scan time).

Cross-sectional skin images (**Fig.1f** revealed the epidermis, dermis, capillary loops and the horizontal plexus of the dermis (**see Suppl Note. 1** for skin-layer representation). Images herein reached ~ 1.5mm depth at the 532nm shown and ~5 mm in the near-infrared. Coronal plots of the 3D volume images depicts the superficial skin ridges in the epidermis layer (**Fig. 1g**), top view of the capillary loops in green (**Fig. 1h)** and dermal vasculature in the vascular plexus (**Fig. 1i).**

The superiority of ultra-broadband detection is shown by contrasting UB-RSOM images to images obtained by conventional optoacoustic imaging at a few tens of MHz band (**see Suppl Note.2**). Even compared to a wide 10-40 MHz range, the UB-RSOM resolution increases by >8x (**Suppl. Fig.2**).

Consequently, **Fig. 1f-i** achieves non-invasive imaging of dermal vasculature, skin layers and capillary loops at detail and resolution to depth ratio that has not been achieved by other modalities. The combination of ultra-broadband and frequency equalization bring therefore never before documented ability in skin imaging.

UB-RSOM of psoriasis and histological validation

A next step was to investigate whether UB-RSOM could resolve and quantify features of psoriasis. 4mm x 2mm affected skin areas from six (n=6) psoriasis patients (**see methods**) were imaged (**Fig.2a**), revealing marked changes compared to healthy skin (**Fig.2b**). The scan time was 70 seconds. Elongated and dilated capillary loops, visualized by Frequency Band Equalization (FBE; Eq.2) in green, could be clearly seen climbing through rete ridges to virtually the skin surface. The layered arrangement observed in the healthy skin disappears in psoriasis and prominent skin acanthosis could be measured by observing the distance from the skin surface to the horizontal vascular plexus. Dermal vessel diameter increased over healthy skin and shows a denser appearance, which is also seen in three-dimensional skin visualizations shown in **Suppl. video 1** and **Suppl. video 2,** for healthy and psoriatic skin respectively. Coronal images visualizing the top part of the capillary loops (**Fig.2c**) were markedly different to UB-RSOM images of healthy skin (**Fig.2d**). Histological H&E analysis of biopsied specimen were contrasted to the corresponding UB-RSOM cross-sections for psoriatic and healthy skin (**Fig.2e,f**) and confirmed the epidermal thickening, capillary elongation and increased dermal vascularization visualized by label-free UB-RSOM *in-vivo*. Quantitative comparison (see **methods**) of the mean epidermal thickness seen in UB-RSOM and histology observed a good match for healthy epidermis thickness (~ 138μm) and psoriatic epidermis (~203 μm) (**Fig. 2g,h**). Excellent match was found between the diameter of individual vessels in the deep dermis (n=9), characterized by CD31 staining and corresponding vessels seen by UB-RSOM image (**Fig.2i,j,k**).

Calculation of UB-RSOM vascular and epidermal features in psoriatic patients and their clinical relevance.

Cross sectional images from different patients revealed marked differences in disease manifestation (Fig.3a,b). A next goal of the study was therefore to quantify pathophysiological features of psoriasis appearing in the study group. UB-RSOM cross sectional images and 3D reconstructions were examined for morphological skin alterations, capillary loop elongation, acanthosis, and changes in dermal vasculature. We computed the (1) total blood volume in the dermis, (2) the fractal number of the vascular structure, (3) the thickness of the epidermis, (4) the density of the capillary loops and (5) the mean diameter of the capillary loops (*see methods*). These measurements were interrogated as label-free biomarkers corresponding to clinically related indications, explained in the following.

The total blood volume (TBV) relates to the "flush" of the inflammatory phenotype. TBV values were computed as the number of voxels in the dermis that corresponded to the inner lumen of blood vessels, based on image segmentation (**see methods**). Each psoriatic lesion exhibited a higher TBV values compared to the adjacent healthy skin. The mean TBV values for psoriatic and healthy skin were 0.11±0.02 mm^3 and 0.071±0.02 mm^3 respectively (**Fig. 3c).** A paired t-test and a Wilcoxon signed ranked test showed significant differences between the total blood volume in healthy skin vs. adjacent psoriatic areas ($p<0.01$ and $p<0.05$ respectively). For comparing areas of different sizes, we defined the blood volume per skin surface (mm) metric, i.e. TBV/Area, where "Area" was defined as the total area scanned by UB-RSOM.

The fractal number of the vascular structures was computed as a second label-free landmark of chronic inflammation and measures vascular spatial complexity associated with vascular changes and aberrant angiogenesis. The higher the fractal number the higher the spatial complexity[19]. The psoriatic skin exhibited a higher mean fractal number of 1.58± 0.06 (a.u) over 1.49±0.09 (a.u) for healthy skin (**Fig. 3c).** A higher

fractal number over healthy skin was also calculated on a per lesion basis (**Fig. 3c).** A paired t-test and a Wilcoxon signed ranked test showed significant differences between the fractal number of healthy skin vs adjacent psoriatic areas ($p<0.01$ and $p<0.05$ respectively).

A third inflammatory landmark related to the psoriasis-associated thickness of the epidermis, which also exhibited marked differences between psoriatic and healthy skin **(Fig. 3c)**. The mean value for psoriatic and healthy skins were 371±102 μm and 108 ± 27 μm respectively; although lesion thickness in individual patients exhibited marked differences (see **Fig. 2h**). The mean thickness difference (acanthosis) between psoriatic and healthy skin was 263±122 μm **(Fig. 3c)**. A paired t-test and a Wilcoxon signed ranked test showed significant differences between the thickness of the epidermis in healthy skin and adjacent psoriatic areas ($p<0.01$ and $p<0.05$ respectively).

We further analyzed the appearance and density of capillary loops, indicative of chronic inflammation and skin reconstruction**.** Capillary loops of the psoriatic skin were clearly detected in the 15-120MHz window exhibiting a mean diameter value of 33±4μm (**Fig.3d**). The mean density of capillary loops in the psoriatic plaques was 21±6 capillaries per mm^2. Characteristically, the capillary loops in healthy skin are smaller in diameter and are not visible in the 15-120MHz window but only when >120 MHz frequencies are employed (**Fig.1f,h**). This finding serves as an example on how spatial frequency patterns can be employed to differentiate conditions and disease.

Finally we interrogated the clinical relevance of the UB-RSOM features by suggesting a new index of optoacoustic features (OPIND), which could quantitatively summarize psoriasis features and severity. The OPIND exhibited strong correlation with the PASI index (see **Fig. 3e,** and "Calculation of the Optoacoustic index (OPIND)" in methods**).**

DISCUSSION

In addition to measuring genomic and environmental variability, precision medicine requires methods that sense and quantify individual disease conditions and responses from patients. Effective clinical application necessitates label-free, non-invasive approaches for capturing patho-physiological phenotypes. Such methods allow longitudinal dissection of biology without perturbing the disease measured. The combination of ex-vivo analytics with *in-vivo* measurements could lead to improved disease prevention, early diagnosis and treatment.

UB-RSOM offers an approach to quantifying skin morphology and inflammatory landmarks not available to other dermatology modalities today, due to ultra-short illumination, ultra-broadband $LiNBO_3$ detection and tomographic reconstruction using high-numerical aperture data collection. UB-RSOM-resolved light absorption contrast allowing a direct and high sensitive detection of vascular structures (hemoglobin) and melanin structures imparting a alternative pathophysiology picture. As shown in **Suppl Note**. **2**, the broad bandwidth is essential in achieving the imaging performance shown. Optoacoustic imaging of the skin has been previously considered with limited bandwidth[13,20], which as shown in **Suppl Fig. 2** yields >100 μm resolution, performance not appropriate for retrieving the fine features visualized herein[21,22-25]. UB detection enabled herein an axial resolution of 4.5 μm and a lateral resolution of 18.4 μm which generally remains approximately constant through the whole dermis (1.5 mm deep) and slightly degrades in deeper layers, reaching ~23μm lateral resolution seen in fat-layer capillaries situated 2.5 mm deep (see **Suppl Note 4** for details). Repeated measurements of the same area were performed and showed that no significant changes are produced in the skin vascular structure by illumination-induced tissue heating.

In addition to the imaging performance shown, a critical finding was the identification of skin features enabling not only morphological inspection but also the interrogation of inflammatory and angiogenic

features, not resolved by current dermatology imaging techniques.Vascularization of the dermis is suspected to play a key role in psoriasis development[4,8] but has so far remained invisible *in-vivo.* . Likewise a larger number of disease biomarkers (epidermis thickness, blood volume density and diameter of capillary loops) were summarized into the OPIND to serve as a quantitative measure of disease severity. Pilot comparison between OPIND and PASI revealed good correlation, even though some changes between the two indices are expected since OPIND resolves three-dimensional features whereby PASI only observes the surface appearance of disease. We expect that the concept of OPIND, possibly after refinement, can offer a quantitative and objective report of inflammatory skin disease, improving upon the subjective nature of the PASI (or other indices such as the SCORAD). The mean difference in fractal number between healthy and psoriatic skin was only 6%, indicating small changes in the pattern complexity of inflamed vessels compared to blood volume or epidermal thickness changes. Measurements of eczema patients also captured changes in acanthosis, capillary loops density and diameter, and vascular volume (**Suppl Fig.3 a,b,c)**, enabling the possibility of objective clinical evaluation of eczema severity or allergy testing over the "Prick Test", the latter suffering from inter-observer variations [26].

In addition to a small, handheld form factor, portable UB-RSOM was shown insensitive to motion and capable of offering high-resolution images of the skin *in-vivo* in ~minute acquisition times. Therefore even in a prototype format, UB-RSOM achieved scanning features appropriate for seamless integration in the dermatology suite. We expect that the depth and UB-RSOM imaging features provided can lead to improved readings of disease and treatment offering clinical value in dermatology examination. FBE was employed herein to better visualize image features, in particular patterns associated with the high-frequency components collected. We employed a different color for low vs. high frequency component representation aimed at better rendering the contrast coming from the high-frequency part of the ultra-bandwidth information. This representation allows for a quick appreciation of the information

contained at high frequencies and ensures that high-frequency contrast is not masked by low frequency components, typically having stronger intensity. Future steps will include research in alternative image processing and representation schemes and further analyze the implication of FBE and alternative methods on image contrast enhancement. FBE has a potential application in quantifying vasoconstriction and vasodilation. Regarding psoriasis management, a larger clinical study will allow refinement of the OPIND index and validation of its use as an accurate quantitative and user-independent metric of psoriasis severity. UB-RSOM can be more broadly applied to the study and clinical evaluation of inflammatory skin diseases, hair imaging, nevi and skin cancers or cardiovascular disease (**see Suppl Note.3**). These measurements could be combined in the future with measurements of dermal infiltration by inflammatory cells, achieved using optoacoustic contrast agents or through hybrid operation with confocal microscopy.

A key next development is the addition of spectral measurements into a portable UB-RSOM system. Operation at multiple wavelengths is currently limited by unavailability of portable ultra-fast pulsed lasers, achieving pulse widths of 1-3 nanoseconds at sufficient energy. Spectral RSOM imaging has been recently shown possible in healthy skin but at lower resolution and speed compared to the performance achieved herein[27], due to employing slow >10-nanosecond width optical parametric oscillator lasers, which are moreover bulky and very expensive for clinical use in dermatology. Progress in ultrafast laser technology is essential for adding spectral capacity to UB-RSOM and enhance skin interrogation by allowing measurements of oxygenation and separation from melanin contributions.

Overall, the quantitative assessment of psoriatic and inflammatory biomarkers heralds new possibilities in the understanding of processes involved at the onset and progression of disease as well as in the longitudinal

monitoring of treatment options. UB-RSOM has therefore the potential to enable quantitative and objective measurements of inflammatory landmarks.

METHODS

Handheld UB-RSOM system

The UB-RSOM system developed is based on a custom-made spherically focused LiNbO3 transducer constructed to yield broadband measurements ranging from 10 MHz to 180 MHz (Fig.1a). Typically, measurements were performed in the 10-180MHz or 10-120MHz band. The 10-180 MHz band is important for resolving sub-15Micron features; such as the capillary loops in the healthy skin (**Suppl Note. 2**). The active element of the transducer has a diameter of 3 mm and a focal distance of 3 mm, leading to an f-number of 1. The detected optoacoustic signals are pre-amplified by a low noise amplifier (63 dB, AU-1291, Mited Inc.). The transducer is scanned perpendicular to its axial axis conforming a rectangular grid parallel to the skin surface, keeping the focal point slightly above the skin surface.

In the scanning head, the transducer is attached to two motorized stages (sized: 35 mm x 35 mm x 15 mm Physik Instrumente GmbH & Co. KG, Karlsruhe, Germany). Illumination was delivered by a customized fiber bundle (CeramOptec Industries, East Longmeadow, USA) that ends in two arms (**Suppl Fig. 1a**). At the bundle ends individual fibers are arranged in a 6.5 mm x 2 mm rectangle (**Fig.1a**) and illuminate a total surface of ~8x8 mm. Inside the illuminated surface a virtually homogeneous rectangular illumination pattern of 8 mm x 5 mm is achieved. The bundles are fixed to an ergonomic casing made of Acrylonitrile Butadiene Styrene build by 3D printing. The illumination light is generated by a 532 nm laser (Bright Solutions, Cura Carpignano, Italy). The temporal width of the pulse is of 0.9 ns and its maximum energy goes up to 1 mJ per pulse. The repetition rate can be selected from single shot up to 2 kHz. An articulated arm helps the user to fix the casing to the imaged area, minimizing motion artifacts in the reconstructed images (Figure 1b and Figure

1c). An interchangeable interface unit (IU) shielded with an optically and acoustically transparent plastic membrane is placed below the casing. The interface unit is filled with 1.5 ml of water and enables the acoustic coupling between the skin and the transducer detection surface. Once the unit is filled, the system is easily placed on top of the desired skin area (**Suppl Fig.1a**). All psoriasis images were generated using optoacoustic signals collected over 4 x 2mm, (266 x 135 scan points) taking a total time of 70 s. The entire patient handling process, including placement of the scanning head on the tissue surface lasted less than 2-3 min. A resolution and sensitivity characterization of the portable UB-RSOM system developed is discussed in the Supplementary Note 4.

Safety limits

According to the American National Standard for Safe Use of Lasers (ANSI, Z136.1-2014) when illuminating a region with light at 532 nm and the exposure time is more than 10 seconds the mean irradiance should not exceed 2000 W/m2. The measured energy per pulse and per area delivered to the sample was of 3.75 μJ/mm2, which imposes a maximum repetition rate of 533 Hz. In order to ensure safety we used a repetition rate of 500 Hz. Within this energy range, the increase of temperature in tissue is of the order of milliKelvin. Control measurements (not shown) demonstrated that there were no alterations in image appearance due to repeated scanning sessions, confirming that there is an absence of UB-RSOM-induced temperature effects on skin physiology.

Image reconstruction, frequency band equalization and rendering

Data were collected in raster scan acquisition assuming an x-y plane parallel to the skin surface. At each position several amplitude mode lines (“A lines”) are obtained in the depth direction, i.e. *z* direction.

The acquired signals are divided in two frequency bands[25,24]: low frequency region (10MHz to 42 MHz) and a high frequency region (40 MHz to 120MHz) for the 10-120MHz implementation. 10-60Mhz and 60-180Mhz bands were alternatively used in the 10-180 MHz implementation (see Methods, Handheld UB-RSOM system for the utility of the different implementations). Signals in the two different bands were independently reconstructed, a process necessary to reduce noise especially in relation to reconstructing high frequency data. Reconstructions were based on a beam forming algorithm [28], which generated three-dimensional images. The beam-forming algorithm has been accelerated by parallelized computing on a GPU, and improved by incorporating the spatial sensitivity field of the detector as a weighting factor into the algorithm[29] .The voxel size of the reconstruction grid was chosen to be 10 µm x 10 µm x 3 µm.

The two resulting images x_{low} and x_{high} correspond to the low and high frequency components of the signal, respectively (**Fig. 1d,e**). A weighting factor α is introduced for modulating the intensity of the high-frequency band image :

$$x_{high}^{p} = \alpha x_{high} \quad (1)$$

Where x_{high}^{p} is the new high frequency band image. A composite image (x_{RGB}) is then constructed by fusing x_{low} into the red channel of an RGB image and x_{high}^{p} into the green channel of the same RGB image (**Fig. 1f-i**). Then contrast between the red and green channel is maximized by solving the following minimization problem.

$$\min_{\alpha} \left\| x_{low} - \alpha x_{high} \right\|^{2} \quad (2)$$

Representing α vs $\left\|x_{low} - \alpha x_{high}\right\|^2$ leads to a function with a clear parabolic shape whose minimum can be calculated simply by brute force minimum search (**see Suppl Note. 1**).

UB-RSOM images can then be rendered by taking the Maximum Intensity Projection (MIPs) of the reconstructed images along the direction shown. In cross-sectional images the entire volume was rendered. In coronal views, the MIP is shown from the reconstructed image within the limits of the layer shown along the z direction (depth).

Patient selection, skin biopsies, data grouping and general statistics

Thirteen psoriasis patients were imaged following approvals from the Ethics Committee of the Klinik und Poliklinik für Dermatologie und Allergologie am Biederstein, Munich Germany. 6 mm skin punch biopsies from skin lesions and clinically non-involved skin were taken of all patients. Before obtaining biopsies, patients gave their written informed consent. Consent for publishing skin photos was also obtained (**Fig. 2,c** and **d**). Biopsies were evaluated by an experienced pathologist to confirm the clinical diagnosis. CD31 immunostaining was also performed to evaluate vessels footprints.

The patients were split into two groups. Group A consisted of six patients of 52-years mean age. The data obtained from group A was used to evaluate UB-RSOM performance as shown in Fig.2 and find psoriasis biomarkers as shown in Fig.3. In order to assess the significance of the statistical differences for the metrics used to compare healthy and adjacent psoriatic skin, we performed both a paired t-test and a Wilcoxon signed rank test. Performing both tests ensures that the samples follow the required statistical distributions. For every metric the variance between the healthy values and psoriatic values were of the same order in is explicitly shown. The selection of the healthy and psoriatic skin areas to be imaged was made by professional dermatologists independently from the authors that processed the data.

Group A was also used to calculate the coefficients of the OPIND model as described in "Methods, Calculation of the optoacoustic index".- Group B consisted of eight psoriasis patients of 46 mean age and

was used to validate the OPIND performance as described in "Methods, Calculation of the optoacoustic index".

Two of the thirteen patients were excluded from the study since the moved during acquisition leading to reconstructions with strong artifacts

Quantitative comparison between RSOM images and histological sections

In order to validate the UB-RSOM fidelity with a gold standard, we compared the images obtained from healthy skin and psoriatic skin of a patient with the counterpart histology samples. Values of epidermis thickness were determined based on assigning 6 equidistant points on the skin surface in both the histology and the UB-RSOM images and taking the average distance seen in the 6 measurements. We further measured the diameter of 9 vessels in the psoriatic skin, identified by both UB-RSOM and CD31. The vessels were selected randomly

Calculation of vascular and epidermal features from psoriatic patients.

In order to quantify the skin features related to psoriasis manifestation we define the following gray scale image:

$$x_{gray} = x_{low} + x_{high}^{p} \quad 3)$$

The regions of the skin containing the features to be quantified are typically segmented from the image x_{RGB} leveraging on the additional contrast given by the FBE (see "Frequency band equalization algorithm"). Then, the features are quantified in the equivalent regions of x_{gray}.

To calculate the total blood volume, fractal number and epidermis thickness, the distribution of the epidermis surface is firstly obtained using an in house developed automatic segmentation algorithm. The images are then transformed, obtaining a synthetic representation of the skin in which the epidermis surface is flat, namely

x^t_{gray} and x^t_{RGB}. In x^t_{RGB} the epidermis can be distinguished from the dermis (see **Fig. 2a and 2b**) due to the FBE. Both regions can be manually segmented by defining a plane parallel to the skin surface that splits the image in two cubes. The upper cube contains the epidermis and the lower cube contain the dermis (typically a volume of 4mm x 2mm x 2mm was selected, although the dermis depth varied by patient). The height of the upper cube is taken as the epidermis thickness, and defines the maximum distance from the epidermis surface to the horizontal vascular plexus.

The image of the dermal microvasculature ($x^{t,b}_{gray}$) is obtained by applying a binary mask to the dermis region of the image x^t_{gray}, which sets to 1 the voxels whose value is above a threshold defined as 25% of the maximum voxel value and 0 the rest. The Total Blood Volume is then calculated as $TBV = N * dV$ where N is the number of nonzero voxels and dV is the voxel volume. The fractal number is obtained from applying the box counting method[30] to $x^{t,b}_{gray}$.

The diameter and density of the elongated and dilated capillary loops were calculated only for the psoriatic skin. The calculation was performed by using a coronal view MIP of the epidermis regions of the image x^p_{high}, (from now on x^{pMIP}_{high}) since it displays a map of the capillary loops (see **Fig. 2c**). Firstly, the number of loops ($nloops$) are located by finding the number of connected components of pixels with a constant intensity value t, whose external boundary pixels all have a value less than t, obtaining immediately the density of the capillary loops as well. After applying a 10% threshold to x^{pMIP}_{high}, the mean area (MA) of the capillary loops tip is calculated using the expression $MA = NdV/nloops$ where N is the number of nonzero voxels and dV is the voxel volume. The diameter of the loops is then obtained assuming that the area is a disc.

Calculation of the Optoacoustic index (OPIND)

To further investigate the clinical relevance of UB-OPAM-resolved features we considered a severity index, i.e .

$$\mathrm{OPIND} = a_1 + a_2\mathrm{ivasc} + a_3\mathrm{cdens} + a_4\mathrm{acanth} + a_5\mathrm{strucc}$$

where *ivasc* is the normalized increased vasculature (difference between the total blood volume in psoriatic healthy skin and adjacent healthy skin), *cdens* is the normalized capillary density, *acanth* is the normalized acanthosis (difference between the skin thickness in psoriatic and adjacent healthy skin) and *strcucc* is the normalized structural change i.e the difference between the fractal number of psoriatic skin and adjacent healthy skin. Using data group A we observed a strong correlation between the PASI component "erythema" and the *ivasc* , (corr=0.86). We also observed that the *acanth* values matched the PASI "indurance" value, as estimated by a licensed dermatologist. However, low correlation was observed between other PASI components and OPIND components. For this reason, we assigned $a_3 = a_5 = 0$.

Using the data from Group A as a training set, we calculated the values a_1, a_2, a_4 by perfoming linear regression to the following expression:

$$\mathrm{PASI} = a_1 + a_2\mathrm{ivasc} + a_4\mathrm{acanth},$$

where the PASI index was calculated by summing the "Erythema" and the "Indurance" values. We obtained $a_2 = 2.29$ with standard error $\mathrm{se} = 0.81$ and $p<0.05$ $a_4 = 1.81$ with $\mathrm{se} = 0.3$ and $p<0.01$ and $a_1 = 0$ with $p<0.001$. For pilot validation of the generality of the OPIND index calculated based on the computed a_1, a_2, a_4, we calculated the OPIND values for the patients included in group B, as shown in Figure 3e and we calculated the percentage of variance of the PASI index explained by the OPIND index.

Data availability

The authors declare that all data supporting the findings of this study are available within the paper and its supplementary information. Raw acquired optoacoustic data can be made available upon reasonable request, with permission of the Klinik und Poliklinik für Dermatologie und Allergologie am Biederstein, Munich, Germany.

Code availability

Custom code is available in Github at https://github.com/juanaguir/UB-RSOM.

Acknowledgements

We acknowledge funding from European Grant INNODERM (687866) Horizon 2020 and Deutsche Forschungsgemeinschaft (DFG), Germany (Leibniz Prize 2013; NT 3/10-1)

Author contributions

J.A Designed and developed the imaging system, designed and performed the experiments, processed the data, provided conceptual input and wrote the paper.
M.S Developed the imaging system, performed the experiments, processed the data
N.G Provided conceptual input, performed the histology experiments
M.O Developed the imaging system and perfomed the characterization experiments
A.B Provided conceptual input
K.E Provided conceptual input and designed the experiments
V.N. Provided conceptual input, designed the experiments, supervised and lead the research, wrote the paper
J.A, **M.S**, **M.O**,**A.B** and **V.N** revised the text after the referees comments.

Competing interests

Vasilis Ntziachristos is a shareholder in iThera-Medical GmbH, Munich, Germany.

5. References

1 Nestle, F. O., Kaplan, D. H. & Barker, J. Psoriasis. *New England Journal of Medicine* **361**, 496-509, doi:doi:10.1056/NEJMra0804595 (2009).
2 Horn, E. J. *et al.* Association of patient-reported psoriasis severity with income and employment. *Journal of the American Academy of Dermatology* **57**, 963-971, doi:10.1016/j.jaad.2007.07.023 (2007).
3 Boehncke, W. H. & Schon, M. P. Psoriasis. *Lancet* **386**, 983-994, doi:10.1016/S0140-6736(14)61909-7 (2015).
4 Griffiths, C. E. & Barker, J. N. Pathogenesis and clinical features of psoriasis. *Lancet* **370**, 263-271, doi:10.1016/S0140-6736(07)61128-3 (2007).
5 Oji, V. & Luger, T. A. The skin in psoriasis: assessment and challenges. *Clinical and experimental rheumatology* **33**, S14-19 (2015).
6 Ashcroft, D. M., Wan Po, A. L., Williams, H. C. & Griffiths, C. E. Clinical measures of disease severity and outcome in psoriasis: a critical appraisal of their quality. *The British journal of dermatology* **141**, 185-191 (1999).
7 Marks, R. Measurement of the response to treatment in psoriasis. *Journal of Dermatological Treatment* **7**, 3 (1996).
8 Ryan, C. *et al.* Research gaps in psoriasis: opportunities for future studies. *Journal of the American Academy of Dermatology* **70**, 146-167, doi:10.1016/j.jaad.2013.08.042 (2014).

9 Lacarrubba, F., Pellacani, G., Gurgone, S., Verzi, A. E. & Micali, G. Advances in non-invasive techniques as aids to the diagnosis and monitoring of therapeutic response in plaque psoriasis: a review. *International journal of dermatology* **54**, 626-634, doi:10.1111/ijd.12870 (2015).

10 Archid, R. *et al.* Confocal laser-scanning microscopy of capillaries in normal and psoriatic skin. *Journal of biomedical optics* **17**, 101511, doi:10.1117/1.JBO.17.10.101511 (2012).

11 Alex, A. *et al.* Multispectral in vivo three-dimensional optical coherence tomography of human skin. *Journal of biomedical optics* **15**, 026025, doi:10.1117/1.3400665 (2010).

12 Pan, Y. & Farkas, D. L. Noninvasive imaging of living human skin with dual-wavelength optical coherence tomography in two and three dimensions. *Journal of biomedical optics* **3**, 446-455, doi:10.1117/1.429897 (1998).

13 Zabihian, B. *et al.* In vivo dual-modality photoacoustic and optical coherence tomography imaging of human dermatological pathologies. *Biomedical optics express* **6**, 3163-3178, doi:10.1364/BOE.6.003163 (2015).

14 Blatter, C. *et al.* In situ structural and microangiographic assessment of human skin lesions with high-speed OCT. *Biomedical optics express* **3**, 2636-2646 (2012).

15 Qin, J., Jiang, J., An, L., Gareau, D. & Wang, R. K. In vivo volumetric imaging of microcirculation within human skin under psoriatic conditions using optical microangiography. *Lasers Surg Med* **43**, 122-129, doi:10.1002/lsm.20977 (2011).

16 Errico, C. *et al.* Ultrafast ultrasound localization microscopy for deep super-resolution vascular imaging. *Nature* **527**, 499-502, doi:10.1038/nature16066 (2015).

17 Gutierrez, M. *et al.* High-frequency sonography in the evaluation of psoriasis: nail and skin involvement. *Journal of ultrasound in medicine : official journal of the American Institute of Ultrasound in Medicine* **28**, 1569-1574 (2009).

18 Jetzfellner, T. *et al.* Optoacoustic tomography with varying illumination and non-uniform detection patterns. *Journal of the Optical Society of America. A, Optics, image science, and vision* **27**, 2488-2495, doi:10.1364/JOSAA.27.002488 (2010).

19 Mancardi, D., Varetto, G., Bucci, E., Maniero, F. & Guiot, C. Fractal parameters and vascular networks: facts & artifacts. *Theoretical biology & medical modelling* **5**, 12, doi:10.1186/1742-4682-5-12 (2008).

20 Favazza, C. P., Jassim, O., Cornelius, L. A. & Wang, L. V. In vivo photoacoustic microscopy of human cutaneous microvasculature and a nevus. *Journal of biomedical optics* **16**, 016015, doi:10.1117/1.3528661 (2011).

21 Braverman, I. M. & Keh-Yen, A. Ultrastructure of the human dermal microcirculation. III. The vessels in the mid- and lower dermis and subcutaneous fat. *The Journal of investigative dermatology* **77**, 297-304 (1981).

22 Aguirre, J. *et al.* Broadband mesoscopic optoacoustic tomography reveals skin layers. *Optics letters* **39**, 6297, doi:10.1364/ol.39.006297 (2014).

23 Schwarz, M., Omar, M., Buehler, A., Aguirre, J. & Ntziachristos, V. Implications of Ultrasound Frequency in Optoacoustic Mesoscopy of the Skin. *IEEE transactions on medical imaging*, doi:10.1109/TMI.2014.2365239 (2014).

24 Omar, M., Soliman, D., Gateau, J. & Ntziachristos, V. Ultrawideband reflection-mode optoacoustic mesoscopy. *Optics letters* **39**, 3911-3914, doi:10.1364/OL.39.003911 (2014).

25 Omar, M., Schwarz, M., Soliman, D., Symvoulidis, P. & Ntziachristos, V. Pushing the Optical Imaging Limits of Cancer with Multi-Frequency-Band Raster-Scan Optoacoustic Mesoscopy (RSOM). *Neoplasia* **17**, 208-214, doi:10.1016/j.neo.2014.12.010 (2015).

26 Verstege, A. *et al.* The predictive value of the skin prick test weal size for the outcome of oral food challenges. *Clinical and experimental allergy : journal of the British Society for Allergy and Clinical Immunology* **35**, 1220-1226, doi:10.1111/j.1365-2222.2005.2324.x (2005).

27 Schwarz, M., Buehler, A., Aguirre, J. & Ntziachristos, V. Three-dimensional multispectral optoacoustic mesoscopy reveals melanin and blood oxygenation in human skin in-vivo (in press). *Journal of biophotonics* (2015).

28 Omar, M., Gateau, J. & Ntziachristos, V. Raster-scan optoacoustic mesoscopy in the 25-125 MHz range. *Optics letters* **38**, 2472-2474, doi:10.1364/OL.38.002472 (2013).

29 Turner, J., Estrada, H., Kneipp, M. & Razansky, D. Improved optoacoustic microscopy through three-dimensional spatial impulse response synthetic aperture focusing technique. *Optics letters* **39**, 3390-3393 (2014).

30 Foroutan-pour, K., Dutilleul, P. & Smith, D. L. Advances in the implementation of the box-counting method of fractal dimension estimation. *Applied Mathematics and Computation* **105**, 15 (1999).

Figure 1 Skin imaging with portable UB-RSOM imaging system, using color coding of frequency bands: a) Schematic of the operation of UB-RSOM. The transducer is raster-scanned parallel to the skin surface, acquiring signals (A-lines) generated owing to illumination by two fixed fiber bundles. The focal point of the transducer is kept above the skin surface. b) Photograph of the scanning head and the articulated arm. c) Photograph of the scanning head in position ready for data acquisition. d-e) Collected optoacoustic signals are filtered in two frequency bands and reconstructed into two images shown in red and green, representing low and high spatial frequencies respectively. f) UB-RSOM image of healthy skin, generated by a novel frequency band equalization algorithm (FBE: Eq.2), which combines low and high spatial frequencies in a single color-coded image. Different biological structures appear in red or green depending on their spatial frequency content. The epidermis (EP) appears mostly in green, and can be clearly resolved from the dermis (DR). In the dermal vasculature, the capillary loops (CL) can be distinguished from the epidermis and from the vascular plexus in the deep dermis (VP). The bigger vessels appear mainly in red, whereas the smaller vessels appear mainly in green. g-i) Maximum Intensity Projections (MIP) in the coronal direction of the epidermis (g) showing the indents of the skin, f the capillary loop layer (h) and dermis (i) Scale bars: 500 μm

Figure 2 UB-RSOM of healthy skin vs. adjacent psoriatic skin and validation with histology. a) The UB-RSOM cross-sectional image corresponding to psoriatic skin shows the top part of elongated capillary loops (arrow) that climbed almost to the skin surface through elongated rete ridges. Due to FBE processing, the capillaries appear in green and are shown interleaved with widened epidermis structures (EP) due to acanthosis, the latter appearing in red with poor contrast due to loss of pigmentation. Below the epidermis, a dilated and dense vascular structure of the dermis (DR) is resolved (in red). Capillary loops are observed in green and separated from the epidermis (red) and the dilated dermal vasculature (red). Scale bars 200 µm. b) The corresponding UB-RSOM cross section of adjacent healthy skin shows a layered epidermis structure (EP) the vessels in the dermis (DR) are clearly resolved. Scale bars 200 µm. c) Photographs of the top of the psoriatic skin region (left) encompassing an area (dotted box) from which the coronal UB-RSOM slice of the epidermis region was taken (right). The top of the capillary loops appear clearly as green dots. Scale bars 300 µm. d) Photographic pictures of the top of the healthy skin region (left). In the corresponding UB-RSOM coronal view, the superficial skin indents are visible. Scale bars, 300 µm. e) Histology image (left) corresponding to the psoriatic skin and equivalent UB-RSOM cross-section (right). The histology shows the acanthosis, the elongated capillary loops through the rete ridge and the increased vascularization of the dermis. The area inscribed in the doted rectangle and labelled with letter "j" was used for CD31 immunostaining (shown in fig 2j). A profile of a capillary is represented in fig 2k, the profile corresponds to the vertical red line labelled with letter "k". Scale bars 200 µm. f) Histology image (left) corresponding to healthy skin and the equivalent UB-RSOM cross section. Scale bars 200 µm. g) Epidermis thickness of healthy skin measured from the UB-RSOM images and histology images respectively. h) Epidermis thickness of healthy skin and psoriatic skin measured from the UB-RSOM images and histology images respectively. i) Vessel diameters in psoriatic skin measured from the UB-RSOM images and CD31 immunostaining images respectively. j) CD31 immunostaining of the dotted section shown on Fig. 2e e, from which the diameter of a vessel in the dermis well below the capillary loops was measured. k) Profile in the axial direction of a vessel parallel to the psoriatic skin surface situated in the dermis well below the capillary loops. The cross-section shown is indicated on Fig.2e by a red line. Error bars in g–i, standard deviation.

Figure 3 Clinical relevance of UB-RSOM measurements. a-b) Cross sectional UB-RSOM images corresponding to two different psoriatic patients (A6 and A1). The epidermis (EP) thickness is significantly different for both patients. The vascular structure in the dermis (DR), show dilated and tortuous vessels. Scale bars 200 µm. c) Top: measurements of the total blood volume, fractal number and epidermis thickness for psoriatic and adjacent healthy skin (patients A1 to A6). For each of the metrics there is statistical significance between healthy and the psoriatic skin. Error bars, standard deviation. Bottom: Box-and-whisker plots of the differences between measurements for psoriatic skin and healthy skin. The difference in total blood volume refers to increased vasculature, the difference in fractal number to structural changes, and the difference in epidermis thickness to acanthosis. The orange and grey parts correspond, respectively, to data values ranging from the median to the third quartile and from the median to the first quartile. d) Representation of the vascular features corresponding to the capillary loops measured from the UB-RSOM images corresponding to the capillary loops density and their mean diameter. Error bars, standard deviation. e) OPIND index vs PASI index for the validation data set and the test data set. The OPIND index calculated for the data group B using the coefficients obtained from data group A explains 96 % of the variance of the corresponding PASI index. The red segment corresponds to the line that would correspond to the ideal case in which the OPIND index would exactly correspond to the PASI index.

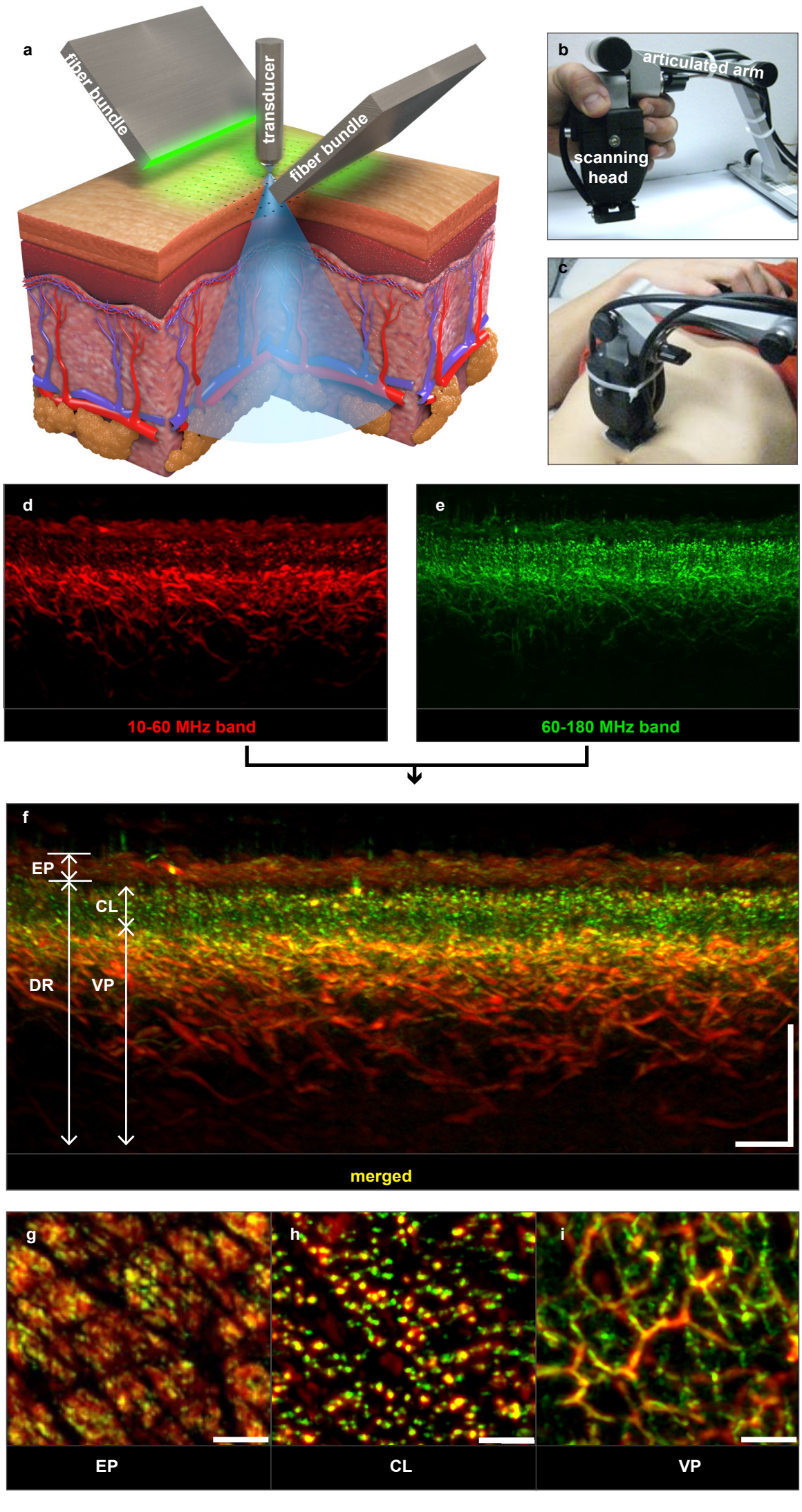
a
fiber bundle
transducer
fiber bundle
b
articulated arm
scanning head
c
d
10-60 MHz band
e
60-180 MHz band
f
EP
CL
DR
VP
merged
g
h
i
EP
CL
VP

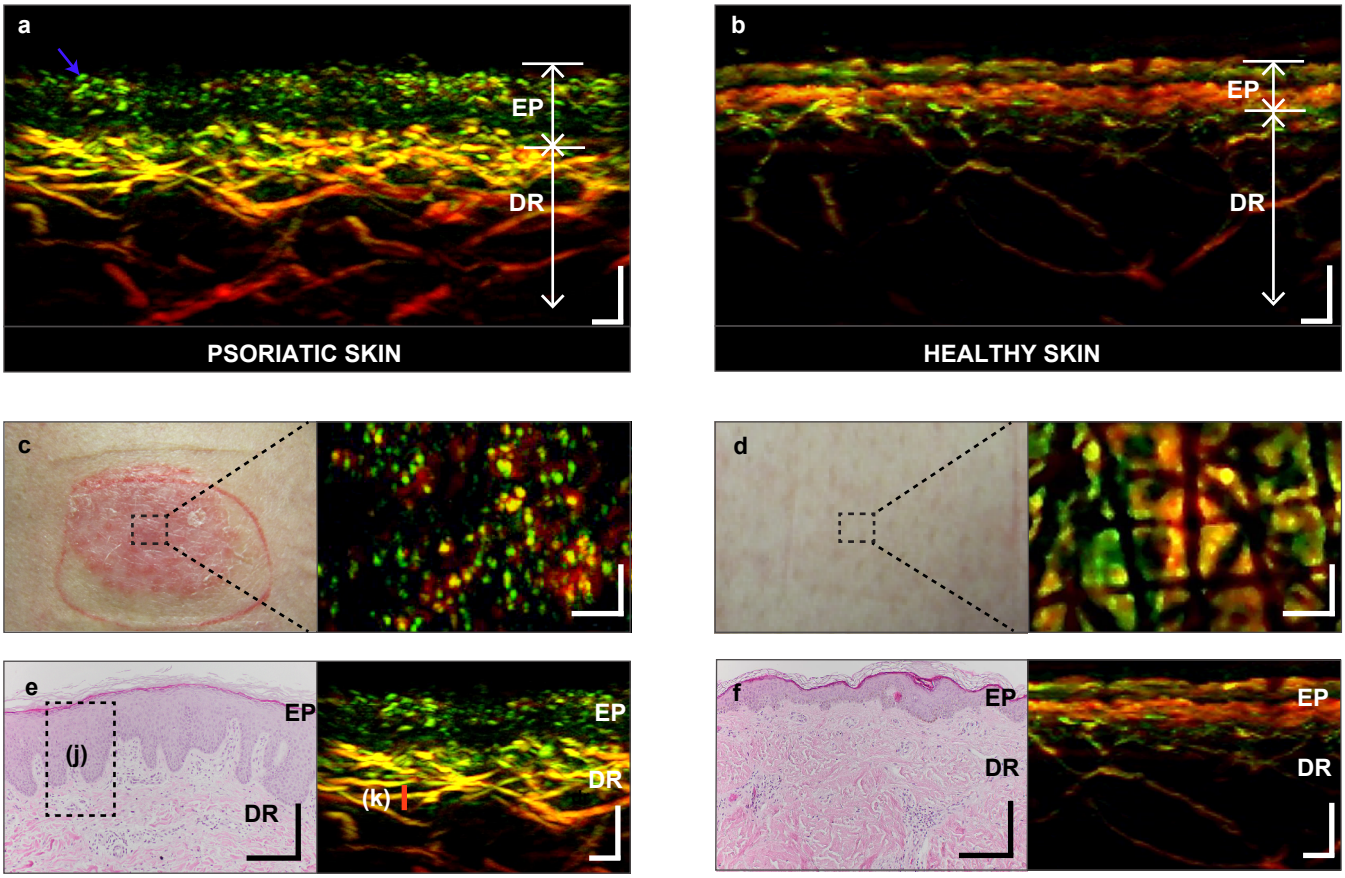
a
EP
DR
PSORIATIC SKIN
b
EP
DR
HEALTHY SKIN
c
d
e
EP
(j)
DR
(k)
EP
DR
f
EP
DR
EP
DR

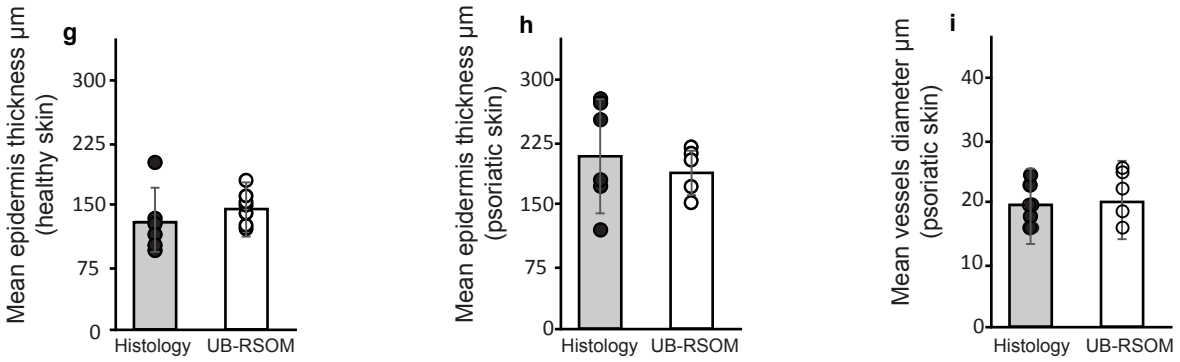
g
Mean epidermis thickness µm (healthy skin)
300
225
150
75
0
Histology
UB-RSOM
h
Mean epidermis thickness µm (psoriatic skin)
300
225
150
75
0
Histology
UB-RSOM
i
Mean vessels diameter µm (psoriatic skin)
40
30
20
10
0
Histology
UB-RSOM

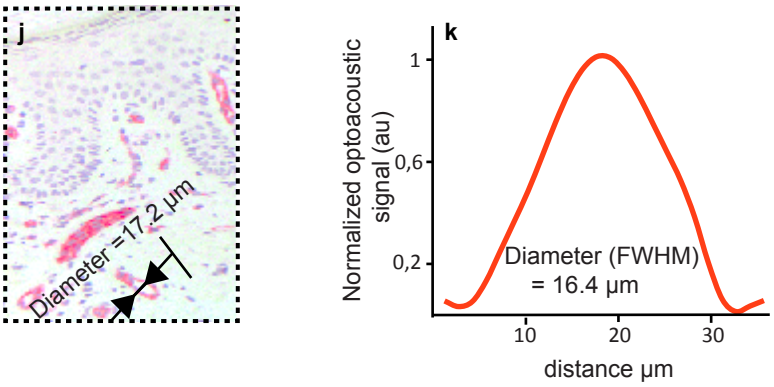
j
Diameter =17.2 µm
k
Normalized optoacoustic signal (au)
1
0,6
0,2
Diameter (FWHM)
= 16.4 µm
10
20
30
distance µm

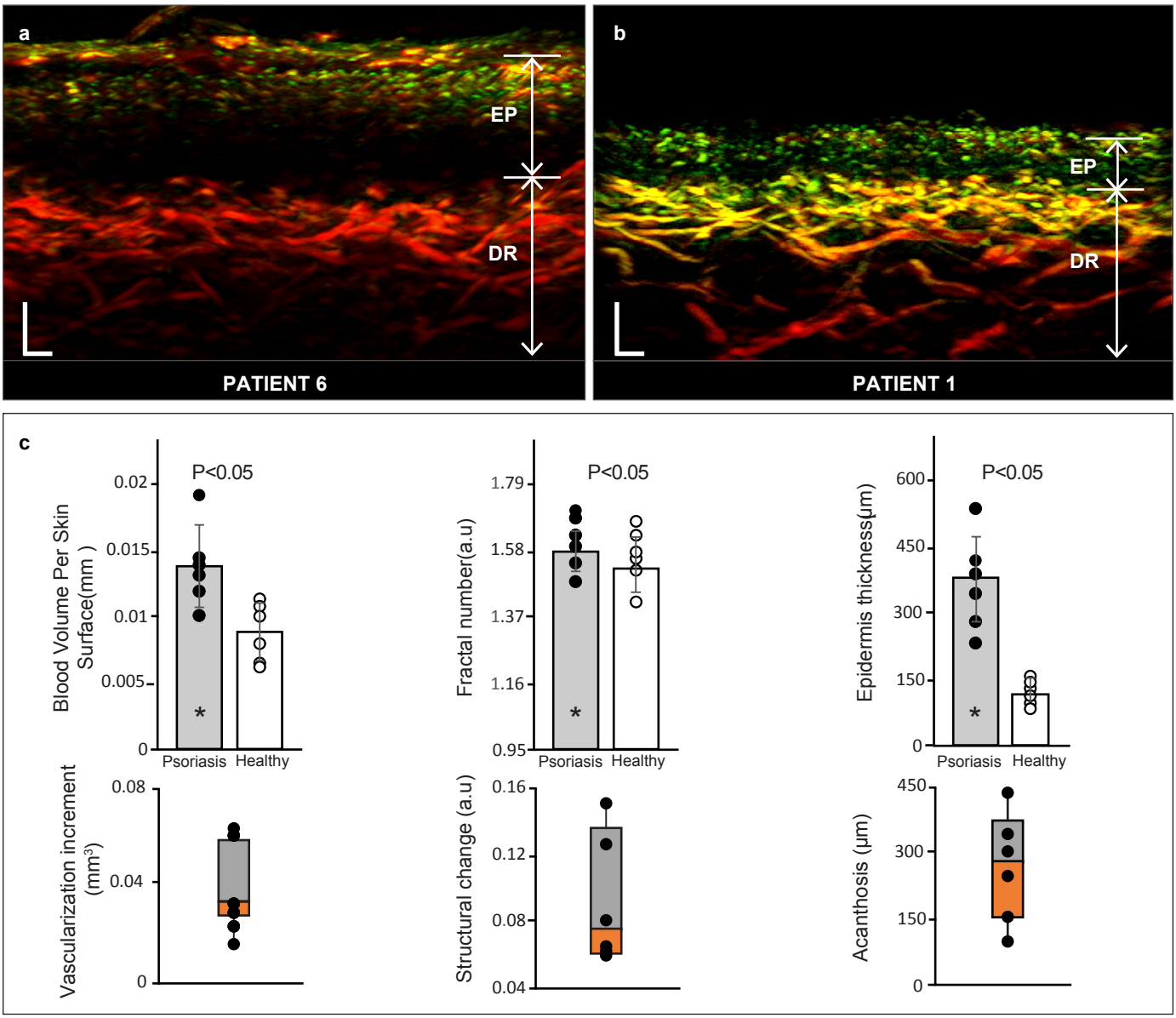
a
EP
DR
PATIENT 6
b
EP
DR
PATIENT 1
c
P<0.05
Blood Volume Per Skin Surface(mm)
0.02
0.015
0.01
0.005
0
Psoriasis
Healthy
P<0.05
Fractal number(a.u)
1.79
1.58
1.37
1.16
0.95
Psoriasis
Healthy
P<0.05
Epidermis thickness(µm)
600
450
300
150
0
Psoriasis
Healthy
Vascularization increment (mm3)
0.08
0.04
0
Structural change (a.u)
0.16
0.12
0.08
0.04
Acanthosis (µm)
450
300
150
0
d
Capillaries per mm2
30
22.5
15
7.5
0
Psoriasis
Capillaries diameter µm
40
30
20
10
0
Psoriasis
e
PASI
6
5
4
3
2
1
1
2
3
4
5
6
OPIND INDEX
GROUP A
GROUP B